

**Hypothalamic perineuronal net assembly is required for sustained diabetes remission
induced by fibroblast growth factor 1 in rats**

Kimberly M. Alonge¹, Zaman Mirzadeh², Jarrad M. Scarlett^{1,3}, Aric F. Logsdon^{4,5}, Jenny M. Brown¹, Elaine Cabrales², Christina K. Chan⁶, Karl J. Kaiyala⁷, Marie A. Bentsen^{1,8}, William A. Banks^{4,5}, Miklos Guttman⁹, Thomas N. Wight⁶, Gregory J. Morton¹, and Michael W. Schwartz^{1*}

¹University of Washington Medicine Diabetes Institute, University of Washington, Seattle, WA, USA.

²Department of Neurosurgery, Barrow Neurological Institute, Phoenix, AZ, USA.

³Department of Pediatric Gastroenterology and Hepatology, Seattle Children's Hospital, Seattle, WA, USA.

⁴Department of Geriatric Research Education and Clinical Center (GRECC), Veterans Affairs Puget Sound Health Care System, University of Washington, Seattle, WA, USA.

⁵Division of Gerontology and Geriatric Medicine, Department of Medicine, University of Washington, Seattle, WA, USA.

⁶Matrix Biology Program, Benaroya Research Institute, Seattle, WA, USA.

⁷Department of Oral Health Sciences, School of Dentistry, University of Washington, Seattle, WA, USA.

⁸Novo Nordisk Foundation Center for Basic Metabolic Research, Faculty of Health and Medical Sciences, University of Copenhagen, Denmark.

⁹Department of Medicinal Chemistry, University of Washington, Seattle, WA, USA.

List of Materials:

Supplementary Figure. 1. Spread of Arc PNNs from normoglycemic Wistar rats span the rostro-caudal length of the mediobasal hypothalamus.

Supplementary Figure 2. Cortical PNNs from normoglycemic Wistar rats exhibit intricate PNN enmeshments encasing both the neuronal soma and extending processes.

Supplementary Figure. 3. Arc PNNs exhibit loose enmeshment coverage of the underlying neurons and lack extracellular HAPLN-1 expression compared to nearby PNN-rich brain regions.

Supplementary Figure 4. Human hypothalamic PNNs exhibit unstructured coverage of the enmeshed neuron compared to tightly structured human cortical PNNs.

Supplementary Figure 5. Diabetic ZDF rats exhibit reduced PNN assembly in ArcM and ArcL areas of the mediobasal hypothalamus.

Supplementary Figure 6. Cortical PNNs from diabetic ZDF rats exhibit intricate PNN enmeshments encasing both the neuronal soma and extending processes.

Supplementary Figure 7. Higher magnification and laser imaging of Arc PNNs in diabetic ZDF rats show the presence of abnormal PNN abundance and distribution throughout Arc.

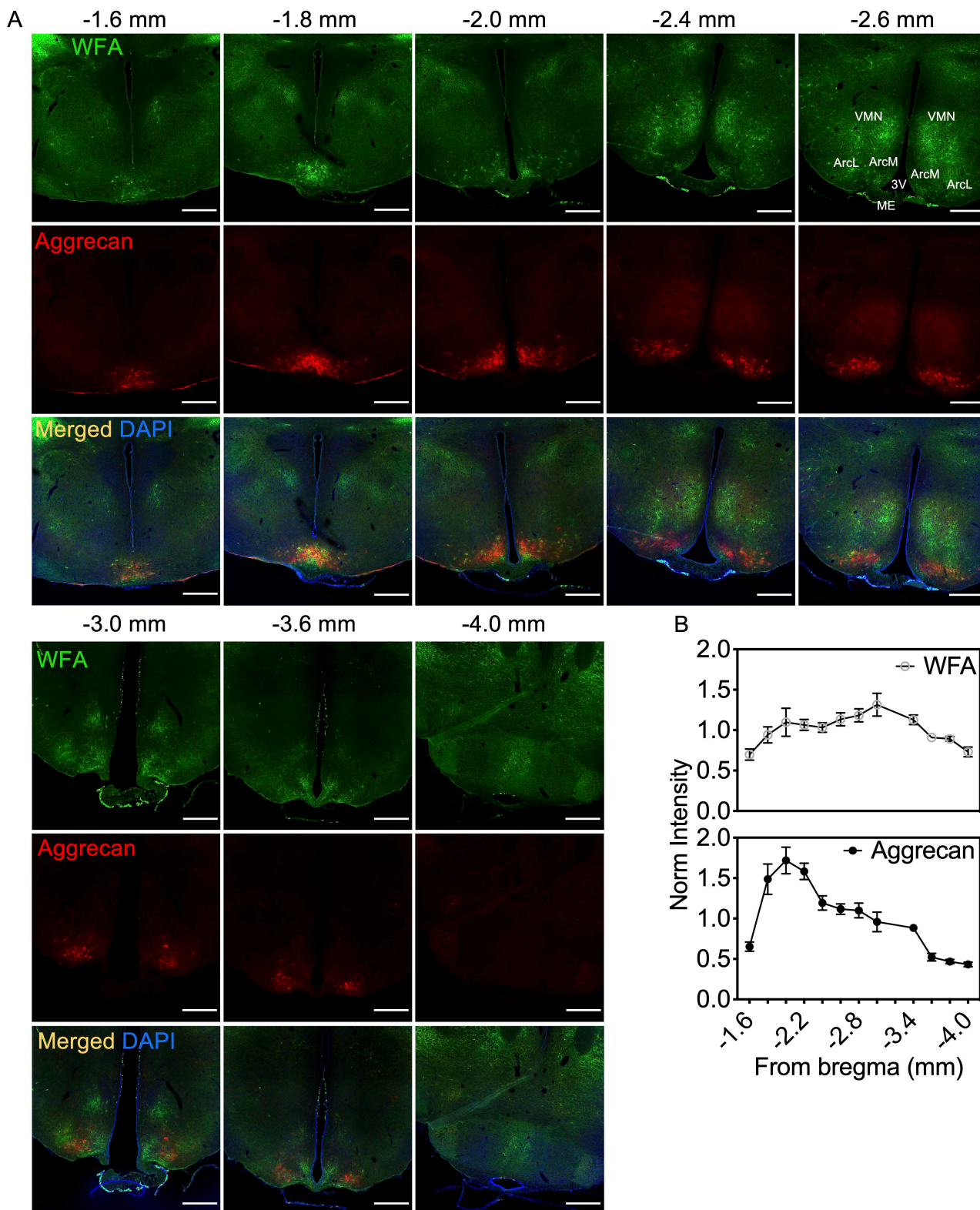
Supplementary Figure 8. Normoglycemic ZDL rats exhibit robust Arc PNNs structures throughout the mediobasal hypothalamus.

Supplementary Figure 9. Hyperglycemia associates with the loss in PNN CS-GAGs in ZDF rats.

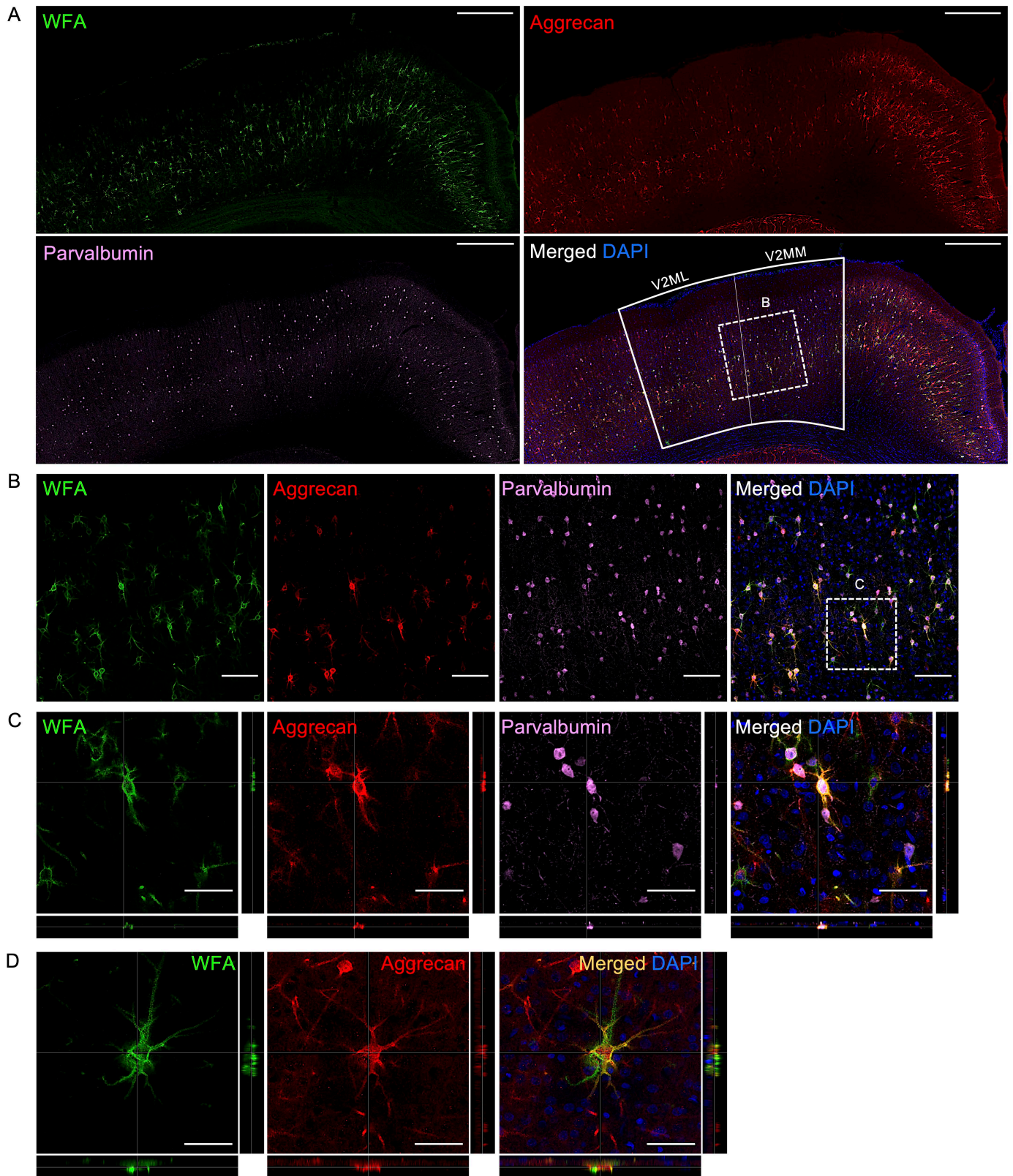
Supplementary Figure 10. Chondroitinase ABC digestion of MBH PNNs *in vivo*.

Supplementary Figure 11. Bilateral PNN digestion by Chondroitinase ABC prevents Arc PNN assembly by icv FGF1 in ZDF rats.

Supplementary Figure 12. Unilateral PNN digestion by Chondroitinase ABC prevents Arc PNN assembly by icv FGF1 in ZDF rats.

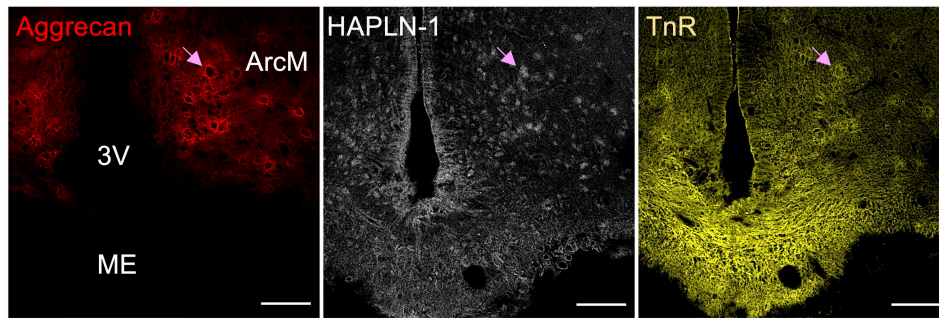


Supplementary Figure 1. Spread of Arc PNNs from normoglycemic Wistar rats span the rostro-caudal length of the mediobasal hypothalamus. A) Imaging of serial coronal sections throughout the Wistar hypothalamus from -1.6 to -4.0 mm posterior from bregma reveals a selective concentration of aggrecan⁺ and WFA⁺ PNN structures in the ArcM and ArcL areas of the mediobasal hypothalamus. Scale bar: 500 μ m. **B)** Quantification and distribution of the total Arc (Arc M+L) mean fluorescence intensity (MFI) of PNNs averaged from hypothalamic sections -1.6 to -4.0 mm posterior from bregma normalized to the Wistar MFI (n=8 rats/group; mean \pm SEM). Arc, arcuate nucleus; ArcL, lateral Arc; ArcM, medial Arc; ME, median eminence; VMN, ventromedial nucleus; 3V, 3rd ventricle.

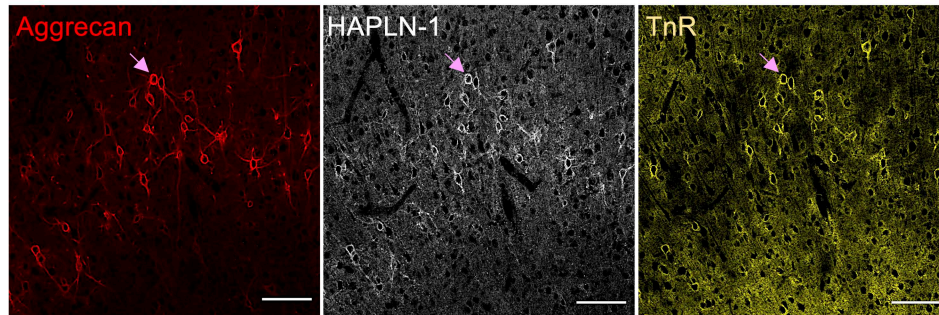


Supplementary Figure 2. Cortical PNNs from normoglycemic Wistar rats exhibit intricate PNN enmeshments encasing both the neuronal soma and extending processes. (A) Tiled panoramic image of a Wistar cortical section containing the mediolateral and mediomedial secondary visual cortex (V2ML and V2MM, respectively) labeled for PNN components (*top, left*) WFA (CS-GAGs), (*top, right*) aggrecan (CSPG), (*bottom, left*) GABAergic inhibitory marker Parvalbumin, and (*bottom, right*) merged image. Scale bar: 500 μ m. (B) Low-magnification view of PNNs in the secondary visual cortex. Scale bar: 100 μ m. (C, D) Higher-magnification orthogonal views of PNN matrix structures in (C) secondary visual cortex and (D) motor cortex. Scale bar: 50 μ m. Images are representative of data from 8 animals.

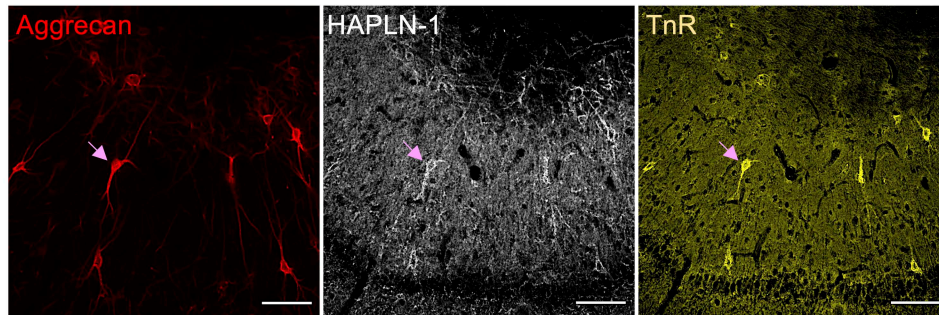
A Hypothalamus



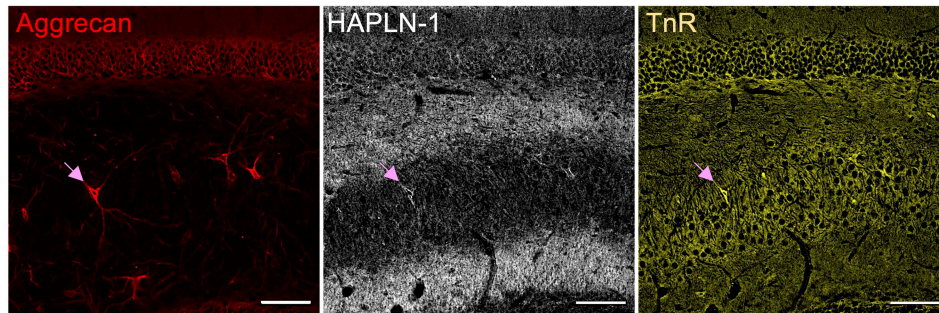
B Cortex



C Fasciola cinereum



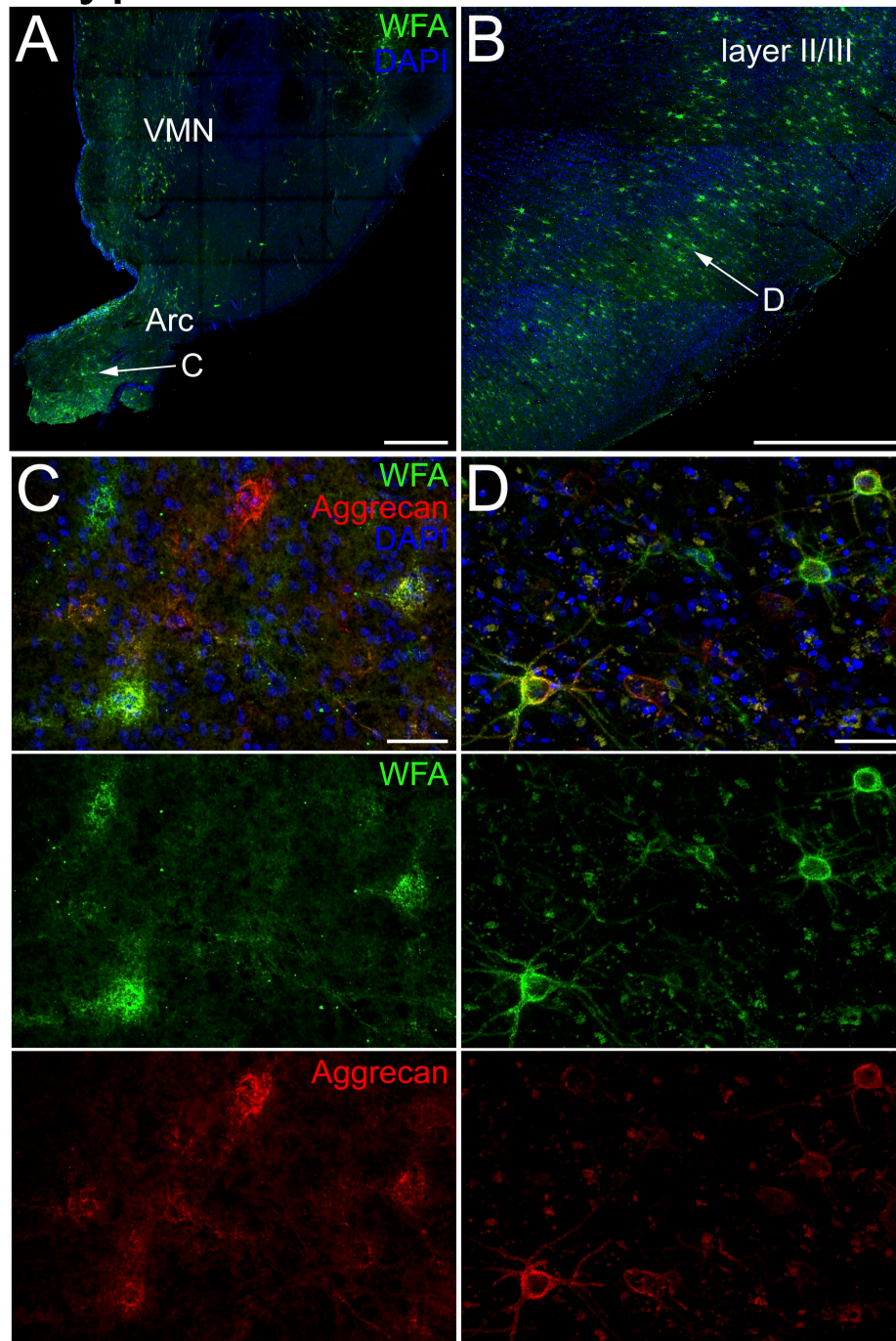
D CA1-Hippocampus



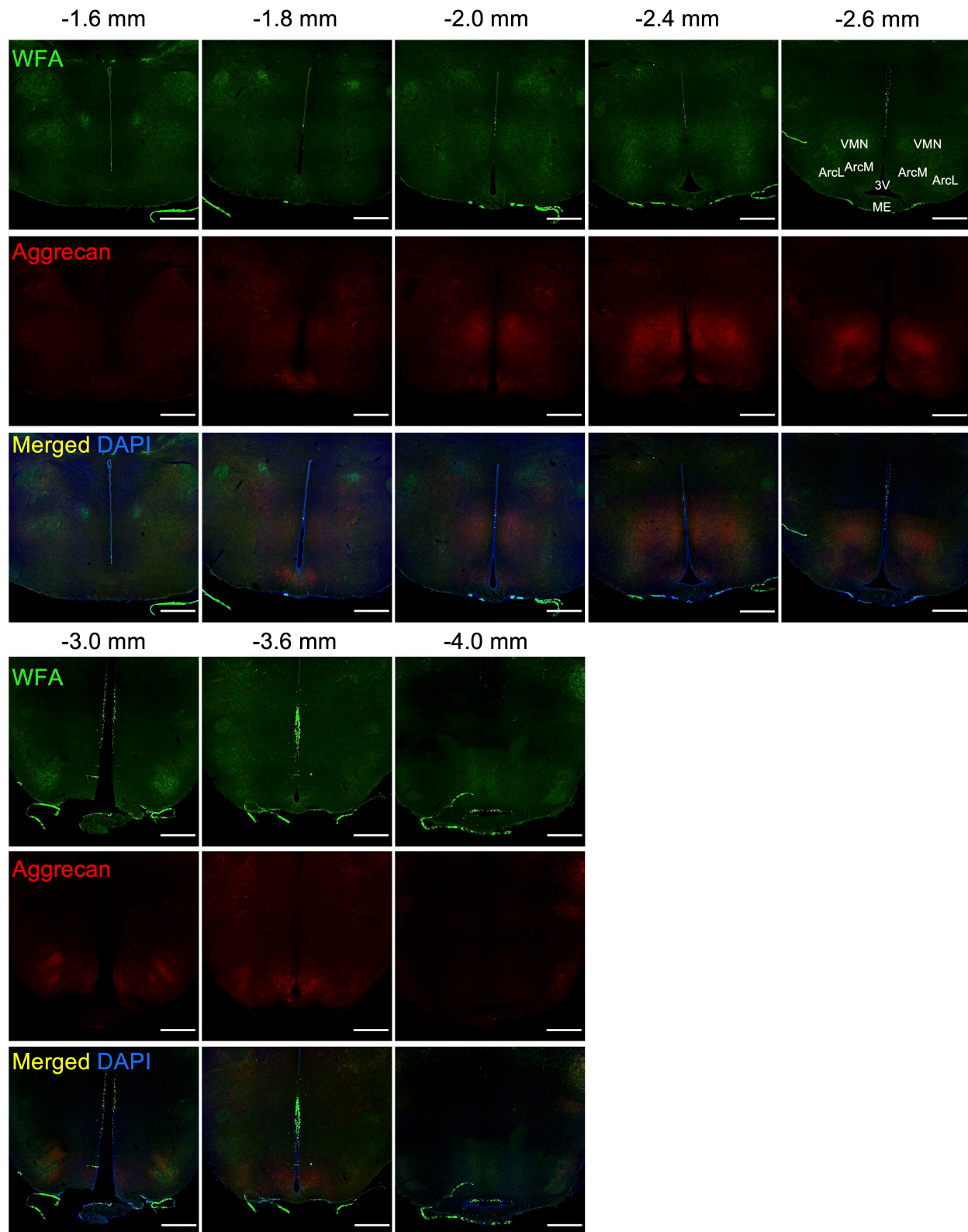
Supplementary Figure. 3. Arc PNNs exhibit loose enmeshment coverage of the underlying neurons and lack extracellular HAPLN-1 expression compared to nearby PNN-rich brain regions. (A) Hypothalamic PNNs in normoglycemic Wistar rats exhibit prominent aggrecan and TnR, but not HAPLN-1, immunoreactivity in the Arc. Unlike the extracellular labeling of aggrecan and TnR, HAPLN-1 labeling in the Arc appears to be intracellular. Nearby PNN-rich regions including (B) cortex, (C) fasciola cinereum and (D) hippocampus of the same animal show PNN matrices are structurally more complex, enmesh both neuronal soma and extending processes, and containing aggrecan, TnR and HAPLN-1 immunolabeling. Scale bar: 100 μ m. Images are representative of data from 8 animals. Arc, arcuate nucleus; ArcM, medial Arc; HAPLN-1, hyaluronan and proteoglycan link protein 1; ME, median eminence; TnR, tenascin-R; 3V, 3rd ventricle.

Hypothalamus

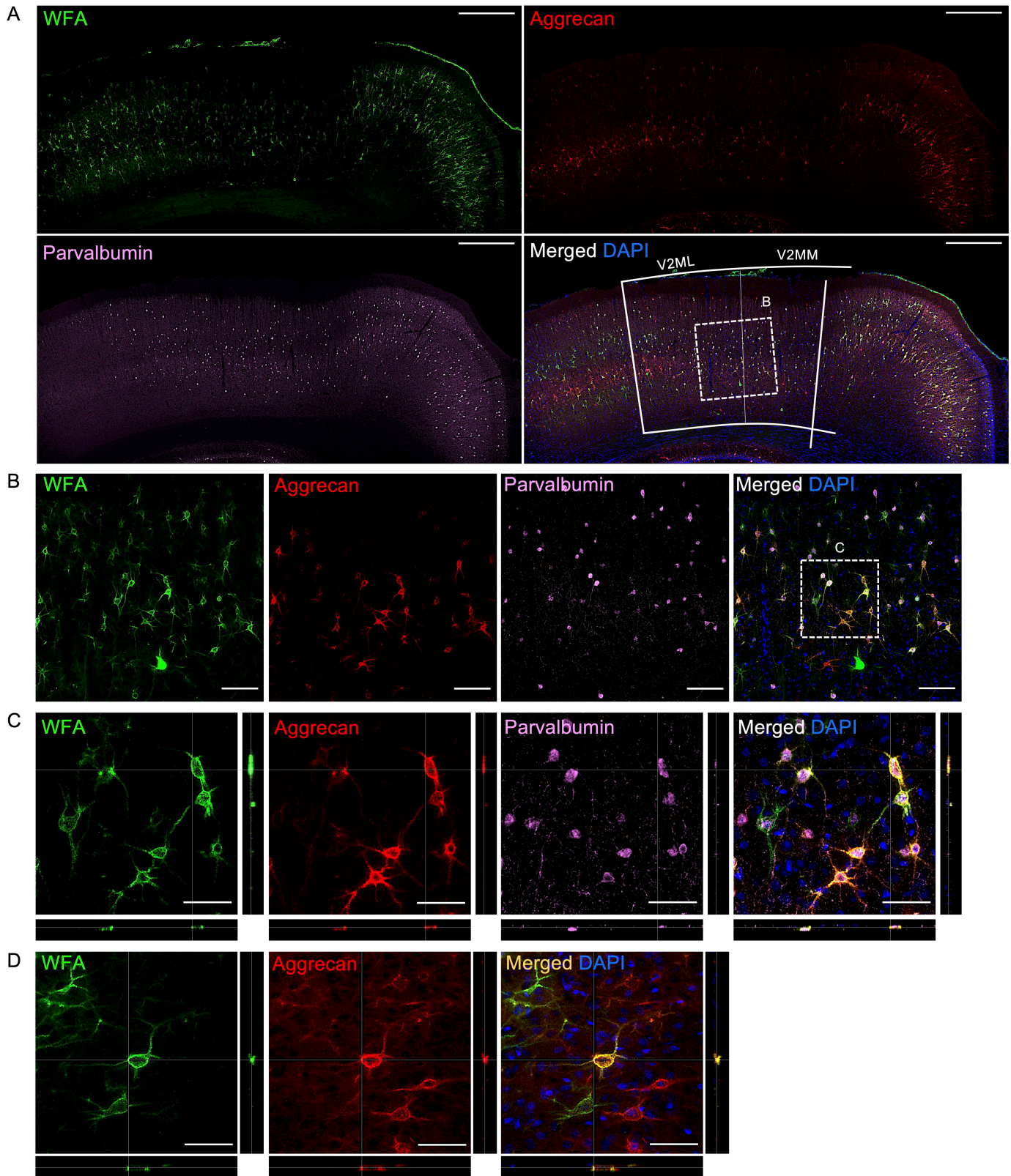
Cortex



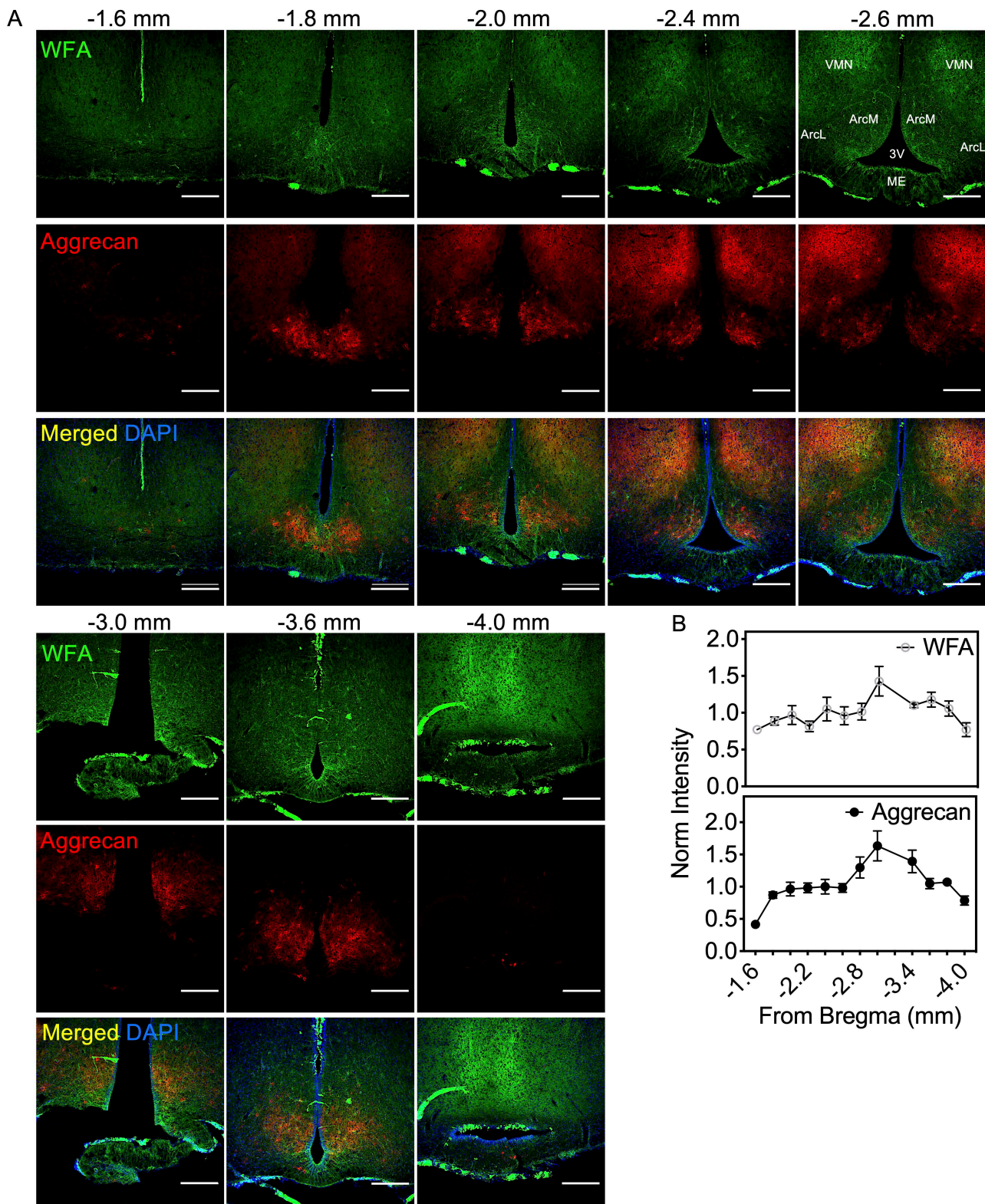
Supplementary Figure 4. Human hypothalamic PNNs exhibit unstructured coverage of the enmeshed neuron compared to tightly structured human cortical PNNs. WFA⁺ / Aggrecan⁺ PNNs in (A, C) human hypothalamus show loose enmeshments surrounding the neuronal soma compared to PNNs in (B, D) human cortex that form intricate lattices surrounding both the soma and proximal processes of the enmeshed neuron. (A,B) Low-magnification tiled panoramic view (Scale bar: 1 mm) and (C,D) higher-magnification view (Scale bar: 50 μ m). PNNs were identified by immunofluorescence in a cohort of human brains (ages 23, 56, 59, 63, and 65 years old) and both the (A, C) hypothalamus and (B, D) cortical images above are from the same 23 yr old donor (please see *Reporting Summary* for additional details). Arc, arcuate nucleus; VMN, ventromedial nucleus.



Supplementary Figure 5. Diabetic ZDF rats exhibit reduced PNN assembly in ArcM and ArcL areas of the mediobasal hypothalamus. Imaging of serial coronal sections through the ZDF hypothalamus from -1.6 to -4.0 mm posterior from bregma reveals a loss in WFA⁺ and aggrecan⁺ PNN structures in the ArcM and ArcL areas of the mediobasal hypothalamus. Scale bar: 500 μ m. Images are representative of data from 8 animals. Immunofluorescence labeling and confocal imaging were performed in parallel to normoglycemic Wistar controls (Supplementary Figure 1). Arc, arcuate nucleus; ArcL, lateral Arc; ArcM, medial Arc; ME, median eminence; VMN, ventromedial nucleus; 3V, 3rd ventricle.

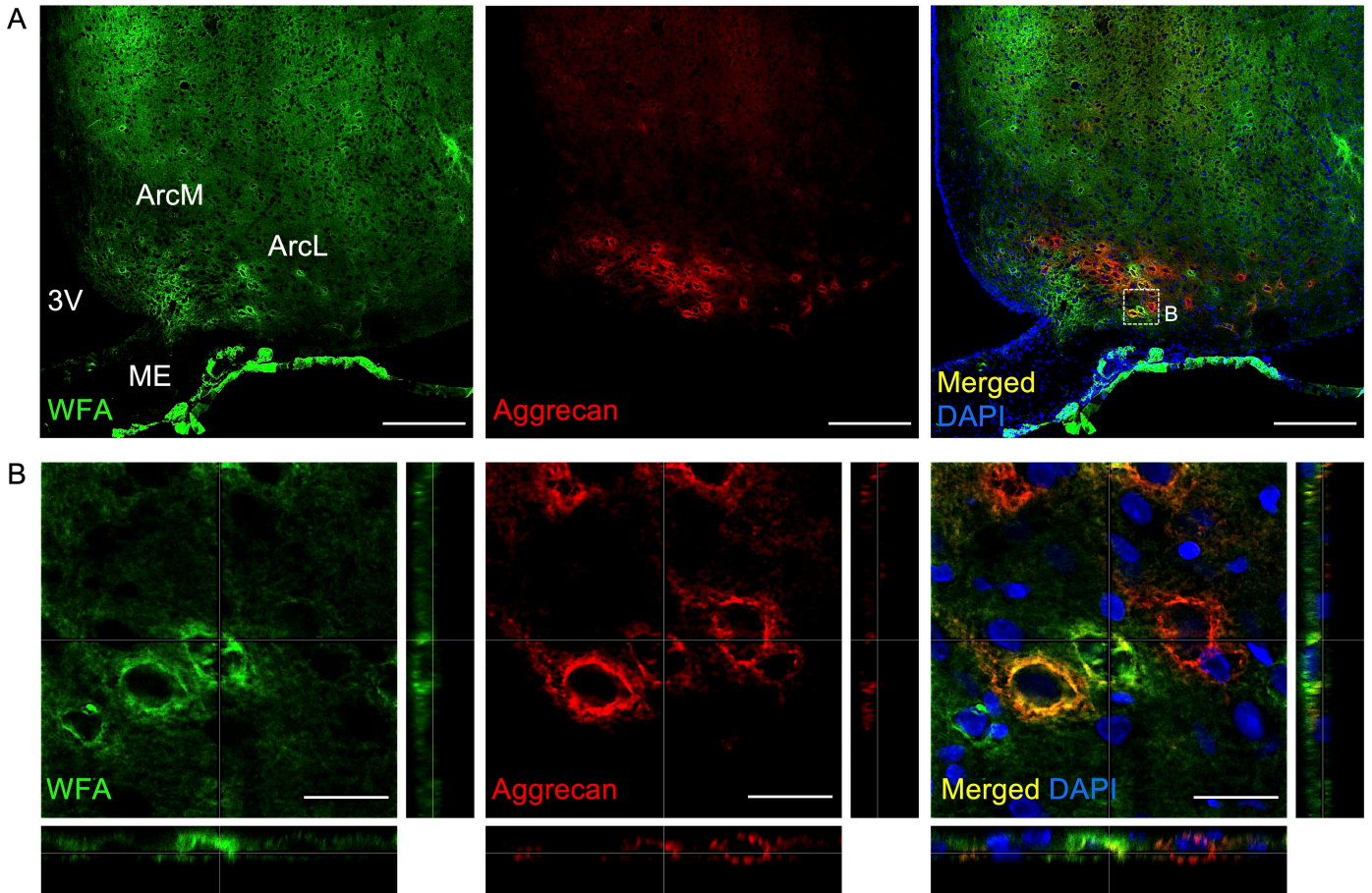


Supplementary Figure 6. Cortical PNNs from diabetic ZDF rats exhibit intricate PNN enmeshments encasing both the neuronal soma and extending processes. (A) Tiled panoramic image of a ZDF cortical section containing the mediolateral and mediomedial secondary visual cortex (V2ML and V2MM, respectively) labeled for PNN components (*top, left*) WFA (CS-GAGs), (*top, right*) aggrecan (CSPG), (*bottom, left*) GABAergic inhibitory marker Parvalbumin, and (*bottom, right*) merged image. Scale bar: 500 μ m. (B) Low-magnification view of PNNs in the secondary visual cortex. Scale bar: 100 μ m. (C, D) Higher-magnification orthogonal views of PNN matrix structures in (C) secondary visual cortex and (D) motor cortex. Scale bar: 50 μ m. Images are representative of data from 8 animals.

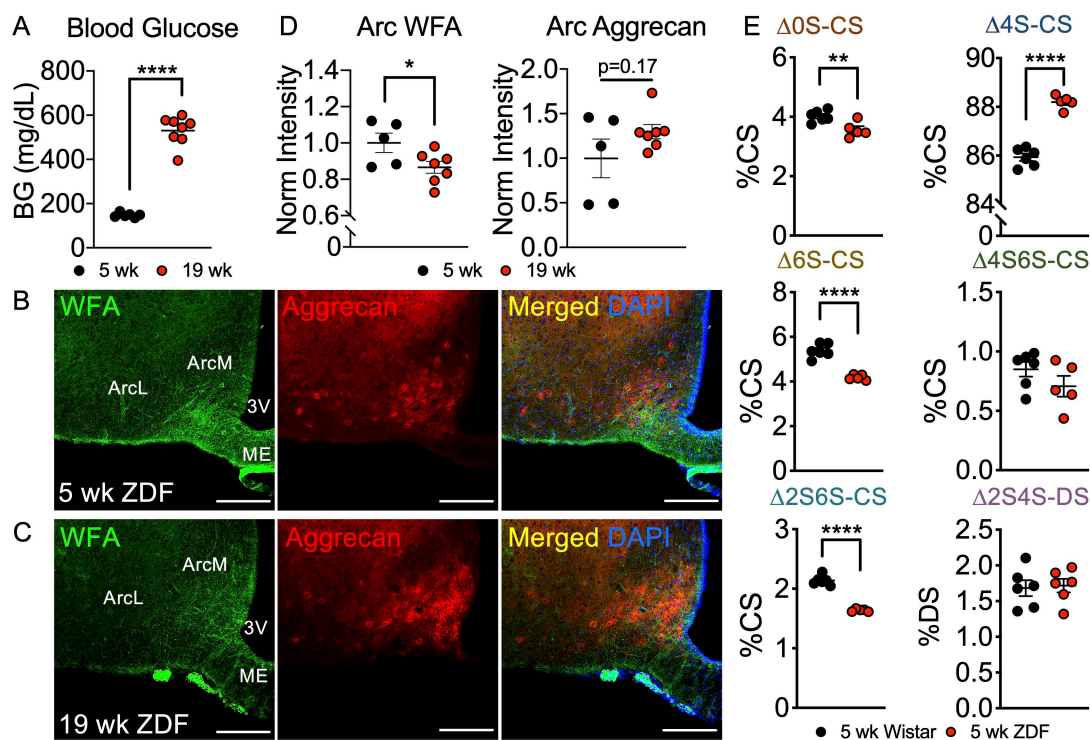


Supplementary Figure 7. Higher magnification and laser imaging of Arc PNNs in diabetic ZDF rats show the presence of abnormal PNN abundance and distribution throughout Arc. A) Imaging of serial coronal sections through the ZDF hypothalamus from -1.6 to -4.0 mm posterior from bregma using enhanced imaging parameters (magnification and laser intensity) show a diffuse-like concentration of aggrecan⁺, but minimal WFA⁺, labeling of hypothalamic PNN structures in the ArcM and ArcL areas of the MBH. The loss of PNNs in the ArcL is somewhat more pronounced than the ArcM region of the MBH. Scale bar: 500 μ m. **B)** Quantification of abnormal distribution of the average total Arc (Arc M+L) mean fluorescence intensity of PNNs averaged from medial hypothalamic sections (-1.6 to -4.0 mm posterior from bregma) normalized to the ZDF mean fluorescence intensity averages (n=8 rats/group; mean \pm SEM). Arc, arcuate nucleus; ArcL, lateral Arc; ArcM, medial Arc; MBH, mediobasal hypothalamus; ME, median eminence; VMN, ventromedial nucleus; 3V, 3rd ventricle.

Normoglycemic ZDLean Rat Hypothalamus

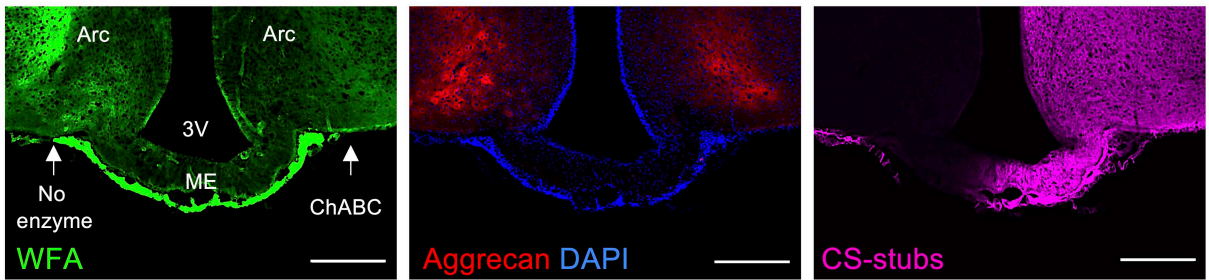


Supplementary Figure 8. Normoglycemic ZDL rats exhibit robust Arc PNNs structures throughout the mediobasal hypothalamus. (A) Low-magnification views (Scale bar: 300 μ m) and (B) higher-magnification orthogonal views (Scale bar: 25 μ m) of WFA⁺ / aggrecan⁺ PNNs in the ArcM and ArcL regions of the mediobasal hypothalamus in ZDL rats. Two separate cohorts of ZDL rats were analyzed, and the results were reproducible between studies. Arc, arcuate nucleus; ArcL, lateral Arc; ArcM, medial Arc; ME, median eminence; 3V, 3rd ventricle.

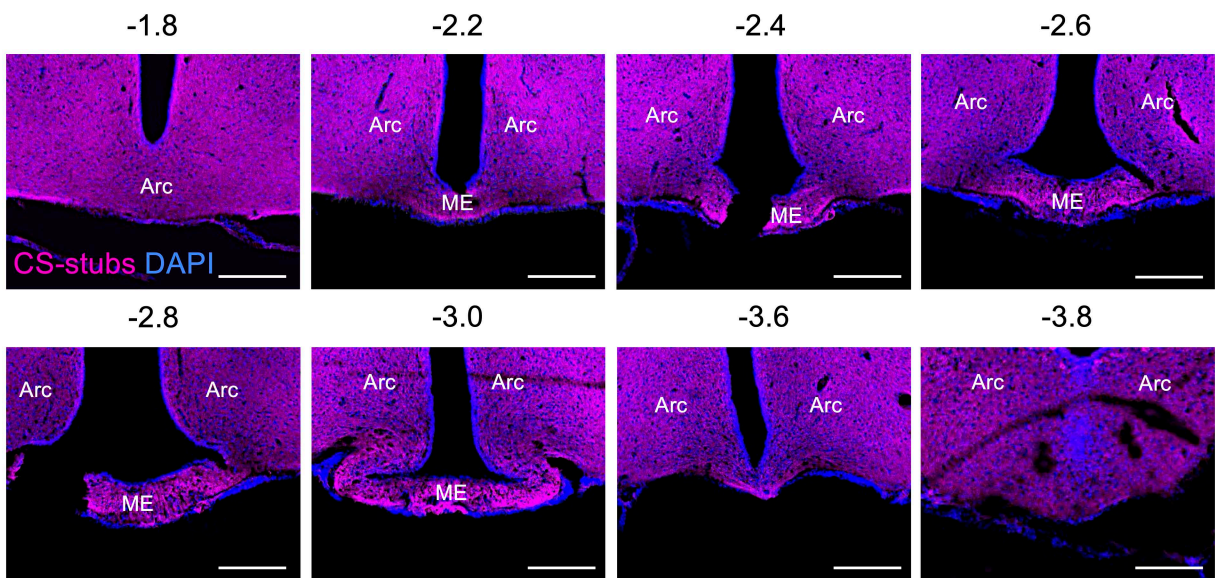


Supplementary Figure 9. Hyperglycemia associates with the loss in PNN CS-GAGs in ZDF rats. Immunofluorescent detection of WFA (PNN CS-GAGs) and aggrecan (PNN CSPG) in coronal sections of rat hypothalamus (30 μ m) between (A) 5 wk old normoglycemic and 19 wk old hyperglycemic ZDF rats show (B-C) loss in Arc CS-GAGs, but not Arc aggrecan, in hyperglycemic 19 wk old ZDFs. Scale bar: 200 μ m. (D) Quantification of the mean fluorescence intensity of PNNs averaged from medial hypothalamic sections (-2.2 to -2.8 mm posterior from bregma) for total Arc (Arc-M+L) areas from 5 wk normoglycemic and 19 wk hyperglycemic ZDF rats and normalized to the 5 wk control mean fluorescence intensity averages. (E) 5 wk normoglycemic ZDF rats exhibit changes in the relative percentages of CS disaccharides compared to age-matched, Wistar controls. *In vivo* measurements (A), immunofluorescence analyses (B-D), and CS/DS-GAG analyses (E) were performed on the same rat cohort (n=5-7 rats/group; mean \pm SEM); * P < 0.05, ** P < 0.01, **** P < 0.0001 versus controls; Student's t-test (unpaired, two-sided); (A) p < 0.0001, (D) p = 0.0470, (E) Δ 0S-CS p = 0.0083, Δ 4S-CS p < 0.0001, Δ 6S-CS p < 0.0001, Δ 2S6S-CS p < 0.0001. Arc, arcuate nucleus; ArcL, lateral Arc; ArcM, medial Arc; ME, median eminence; 3V, 3rd ventricle.

A Wistar- 4 d unilateral ChABC

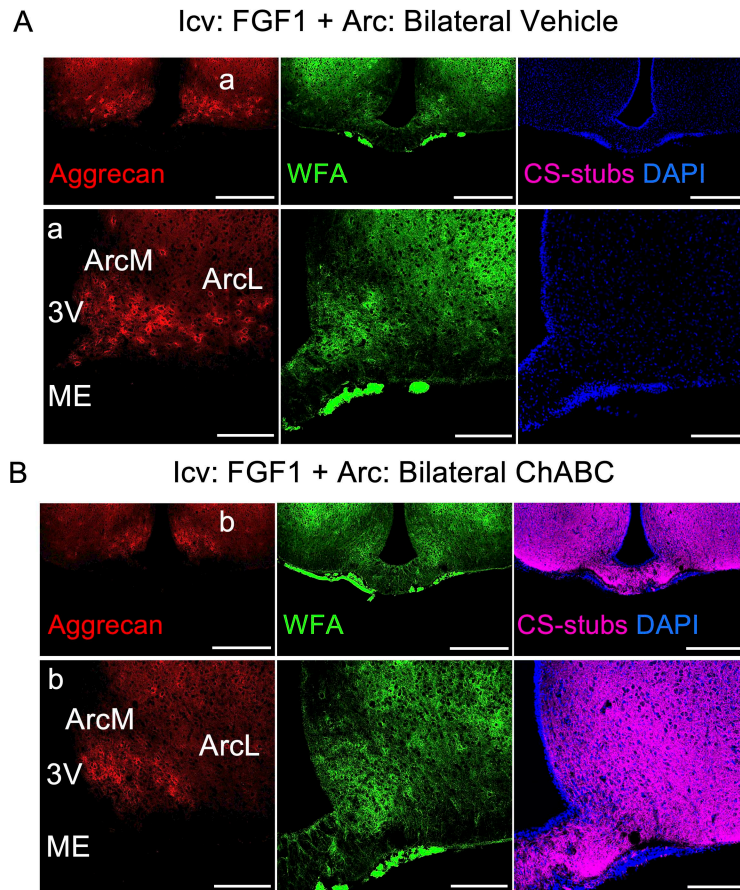


B ZDF- 31 d bilateral ChABC



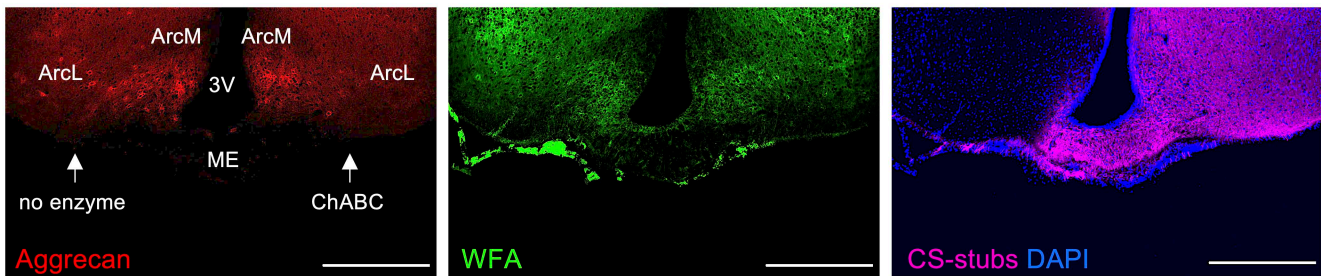
Supplementary Figure 10. Chondroitinase ABC digestion of MBH PNNs *in vivo*.

(A) Immunofluorescent detection of WFA (CS-GAGs), aggrecan (CSPG), and CS-stubs in coronal sections of Wistar rat hypothalamus (30 μ m) after unilateral microinjection of ChABC in normoglycemic Wistar rats and sacrificed 4 d later. Loss of WFA labeling and appearance of CS-stubs confirms successful digestion of PNN-associated CS-GAGs. The decrease in aggrecan⁺ PNN structures shows successful PNN disassembly. **(B)** Bilateral microinjection of ChABC in ZDF rats and sacrificed 31 d later show CS-stub labeling throughout the full rostro-caudal extent of the Arc-ME junction and confirms successful targeting and disassembly of Arc PNNs (Scale bar: 300 μ m). (A-B) Wistar rats were unilaterally microinjected with ChABC and sacrificed at 3 separate time points (4, 7, 14 d; 4 d shown above), and digestion was observed at all 3 time points. Bilateral digestion of hypothalamic PNNs was repeated over 3 separate studies, and the results were reproducible. Arc, arcuate nucleus; ChABC, Chondroitinase ABC; MBH, mediobasal hypothalamus.



Supplementary Figure 11. Bilateral PNN digestion by Chondroitinase ABC prevents Arc PNN assembly by icv FGF1 in ZDF rats. ZDF rats were treated with icv FGF1 and immediately followed by a *bilateral* microinjection of **(A)** heat-inactivated ChABC vehicle control or **(B)** active ChABC targeting the mediobasal hypothalamus within the same surgical session. Immunofluorescence detection of aggrecan (CSPG), WFA (CS-GAGs), and CS-stubs in coronal sections of rat hypothalamus (30 μm) from ZDF rats show ChABC digestion prevented FGF1 stimulated assembly of ArcL PNNs, but not ArcM PNNs, compared to the non-digested, contralateral side. Five ZDF rats were Icv injected with FGF1 and coupled with bilateral Arc injection with heat-inactivated ChABC vehicle, and nine ZDF rats were Icv injected with FGF1 and coupled with bilateral Arc injection with ChABC, over 3 separate experiments, and the results were reproducible. Scale bars: **(A, B)** 500 μm and **(a, b)** 200 μm . Arc, arcuate nucleus; ArcL, lateral Arc; ArcM, medial Arc; ChABC, Chondroitinase ABC; ME, median eminence; 3V, 3rd ventricle.

Icv: FGF1 + Arc: Unilateral ChABC



Supplementary Figure 12. Unilateral PNN digestion by Chondroitinase ABC prevents Arc PNN assembly by icv FGF1 in ZDF rats. ZDF rats were treated with icv FGF1 and immediately followed by a *unilateral* microinjection of ChABC targeting the mediobasal hypothalamus within the same surgical session. Immunofluorescence detection of aggrecan (CSPG), WFA (CS-GAGs) and CS-stubs in coronal sections of rat hypothalamus (30 μ m) from ZDF rats show ChABC digestion prevented FGF1 stimulated assembly of ArcL PNNs, but not ArcM PNNs, compared to the non-digested, contralateral side. Three ZDF rats were unilaterally injected with ChABC over 2 separate experiments, and the results were reproducible. Scale bar: 500 μ m. Arc, arcuate nucleus; ArcL, lateral Arc; ArcM, medial Arc; ChABC, Chondroitinase ABC; ME, median eminence, 3V, 3rd ventricle.